DRAFT VERSION DECEMBER 14, 2023
Preprint typeset using LaTeX style emulateapj v. 12/16/11

RESTORATION OF THE TULLY-FISHER RELATION BY STATISTICAL RECTIFICATION

HAI FU
Department of Physics & Astronomy, University of Iowa, Iowa City, IA 52242
Draft version December 14, 2023

ABSTRACT

Subject headings: Astrostatistics, Scaling relations, Disk galaxies, Galaxy rotation, Galaxy luminosities

1. INTRODUCTION

A wide range of observational problems in astronomy aims at reversing the transformation from distributions of intrinsic properties to those of observed properties. For example, from measurement value to true value in the absence of error or loss of information, from projected shape to intrinsic shape, from reddened magnitude/color to extinction-free magnitude/color, etc. The mathematical formulation of this general problem is based on *the law of total probability*. Suppose the observed properties $(\tilde{x},\tilde{y})$ are transformed from intrinsic properties (ξ,η) and measurement errors (σ_x,σ_y), following a conditional probability density function (PDF) $P(\tilde{x},\tilde{y}|\xi,\eta,\sigma_x,\sigma_y)$, the distribution of the intrinsic properties, $\psi(\xi,\eta)$, and that of the observed properties, $\phi(\tilde{x},\tilde{y})$, are related by the law of total probability:

$$\phi(\tilde{x},\tilde{y}) = \iint \psi(\xi,\eta)P(\tilde{x},\tilde{y}|\xi,\eta,\sigma_x,\sigma_y)d\xi d\eta \tag{1}$$

Usually, the objective is to recover the intrinsic distribution from the observed distribution given the knowledge of the conditional PDF, i.e., to reverse the law of total probability.

Convolution is a special case of Eq. 1 when the conditional PDF can be expressed as differences between intrinsic and observed properties:

$$\phi(\tilde{x},\tilde{y}) = \iint \psi(\xi,\eta)K(\tilde{x}-\xi,\tilde{y}-\eta|\sigma_x,\sigma_y)d\xi d\eta \tag{2}$$

$K(\tilde{x}-\xi,\tilde{y}-\eta|\sigma_x,\sigma_y)$ is called the convolution kernel, and its shape is invariant across the plane of ξ and η. Similar to the general reversal problem, the goal of *deconvolution* is to recover $\psi(\xi,\eta)$ based on the knowledge of $\phi(\tilde{x},\tilde{y})$ and the convolution kernel. One particularly important problem is "image restoration", that is to recover the intrinsic surface brightness map by removing or reducing of the effects of the point spread function (PSF) due to atmospheric seeing and telescope/interferometer geometry. Popular algorithms include RICHARDSON-LUCY (Richardson 1972; Lucy 1974), CLEAN (Högbom 1974; Cornwell 2009), and WIENER-HUNT (Orieux et al. 2010).

Because the conditional PDF does vary across the plane of ξ and η, deconvolution algorithms usually cannot handle the reversal of the law of total probability in Eq. 1. But there is one exception. The iterative rectification algorithm of Lucy (1974) is in fact *designed* to reverse Eq. 1, and that is the main difference between the LUCY rectification algorithm and the RICHARDSON-LUCY deconvolution algorithm.

In this work, I will apply the rectification algorithm to restore the Tully & Fisher (1977) relation, which is a tight power-law relation between absolute magnitude and velocity width for disk galaxies. In numerous previous studies (e.g., Tully & Courtois 2012; Zaritsky et al. 2014; Tiley et al. 2016; Desmond 2017; Topal et al. 2018; Ball et al. 2023), the observed luminosities and velocity widths were corrected using inclination angles estimated from the observed axial ratios (b/a). The rectification technique implemented here eliminates the need of b/a measurements and replaces the highly uncertain individual correction with robust statistical rectification. In §2, I will briefly introduce the rectification algorithm in 1D and 2D. In §3, I will describe the data set in §3.1, construct the joint PDF in §3.2, rectify iteratively the observed distribution in §3.3, and compare the resulting Tully-Fisher relation with that from the b/a-based individual correction method in §3.4. Finally, I will summarize the work and comment on future applications in §4.

2. ALGORITHM

The iterative rectification algorithm of Lucy (1974) was inspired by Bayes' theorem. Given the law of total probability, $\phi(x) = \int \psi(\xi)P(x|\xi)d\xi$, one can define its inverse relation, $\psi(\xi) = \int \phi(x)Q(\xi|x)dx$, with the inverse PDF $Q(\xi|x)$. In other words, given that $P(x|\xi)dx$ is the probability that x' falls in the interval $(x,x+dx)$ under the condition that $\xi' = \xi$, $Q(\xi|x)d\xi$ is the probability that ξ' falls in the interval $(\xi,\xi+d\xi)$ under the condition that $x' = x$. With Bayes' theorem, $\phi(x)Q(\xi|x) = \psi(\xi)P(x|\xi)$, one can replace $Q(\xi|x)$ in the inverse convolution and obtain the following equation:

$$\begin{aligned}\psi(\xi) &= \int \phi(x)Q(\xi|x)dx \\ &= \int \phi(x)\Big(\frac{\psi(\xi)P(x|\xi)}{\phi(x)}\Big)dx \\ &= \psi(\xi)\int \frac{\phi(x)}{\phi(x)}P(x|\xi)dx\end{aligned} \tag{3}$$

At first glance, the above may seem to be trivial as the terms cancel out and the integral of the PDF $P(x|\xi)$ must be unity. But it inspired a highly efficient algorithm that allows the iterative solution of the intrinsic distribution function $\psi(\xi)$ from the observed distribution function $\phi(x)$, when the conditional PDF $P(x|\xi)$ is known. At the r-th iteration, the Lucy (1974) algorithm is simply described by two equations:

$$\phi^r(x) = \int \psi^r(\xi)P(x|\xi)d\xi \tag{4}$$

$$\psi^{r+1}(\xi) = \psi^r(\xi)\int \frac{\tilde{\phi}(x)}{\phi^r(x)}P(x|\xi)dx \tag{5}$$

Evidently, Eq. 4 is the law of total probability, and Eq. 5 is the iterative version of Eq. 3. The only new term is $\tilde{\phi}(x)$, which is the observed distribution function of x and does not change with iterations.

For two-dimensional problems incorporating measurement errors, the iterative equations become:

$$\phi^r(\tilde{x},\tilde{y}) = \iint \psi^r(\xi,\eta) P(\tilde{x},\tilde{y}|\xi,\eta,\sigma_x,\sigma_y) d\xi d\eta \quad (6)$$

$$\psi^{r+1}(\xi,\eta) = \psi^r(\xi,\eta) \iint \frac{\tilde{\phi}(\tilde{x},\tilde{y})}{\phi^r(\tilde{x},\tilde{y})} P(\tilde{x},\tilde{y}|\xi,\eta,\sigma_x,\sigma_y) d\tilde{x} d\tilde{y} \quad (7)$$

where I used $\tilde{x},\tilde{y}$ to denote the measured projected values and use x,y to denote the true projected values (i.e., in the absence of measurement errors).

In brief, the procedure of the algorithm is to:

1. quantify the observed distribution function $\tilde{\phi}(\tilde{x},\tilde{y})$ from the data,
2. define the joint PDF $P(\tilde{x},\tilde{y}|\xi,\eta,\sigma_x,\sigma_y)$ for the particular problem,
3. prescribe an initial guess of the intrinsic distribution function $\psi^0(\xi,\eta)$, and
4. solve iteratively for the intrinsic distribution function $\psi(\xi,\eta)$ with the previous two equations.

In the next section, I will apply the algorithm to recover the Tully-Fisher relation.

3. APPLICATION ON THE TULLY-FISHER RELATION

In this section, I first describe the data set used to construct the observed distribution function, then define the joint PDF, and finally show the deconvolution result. In the following, I define $\tilde{x}$ as the observed projected velocity width (W_{20} in §3.1), ξ the edge-on velocity width, $\tilde{y}$ the observed projected i-band absolute magnitude (M_i in §3.1), and η the face-on i-band absolute magnitude. The goal is to recover the distribution of the galaxy sample in ξ and η, $\psi(\xi,\eta)$, from the observed distribution in $\tilde{x}$ and $\tilde{y}$, $\tilde{\phi}(\tilde{x},\tilde{y})$. Consistent with §2, x and y are reserved for true projected velocity width and true projected i-band absolute magnitude in the absence of measurement error, and they will be integrated out when evaluating the joint PDF of $\tilde{x}$ and $\tilde{y}$.

3.1. *Data*

In this section, I apply the technique to recover the Tully-Fisher relation from the observed distribution of a full sample of Arecibo H I-selected galaxies in the velocity width vs. absolute magnitude space. The H I measurements are taken from the 100% complete Arecibo Legacy Fast ALFA (ALFALFA) catalog (the $\alpha.100$ sample; Haynes et al. 2018) and the absolute magnitudes are from the cross-matched ALFALFA-SDSS galaxy catalog (Durbala et al. 2020). In both catalogs, distances to the galaxies are inferred from Hubble's law with $H_0 = 70$ km s^{-1} Mpc^{-1} and a local peculiar velocity model (for details, see §3 of Haynes et al. 2018). I merge the two catalogs based on the Arecibo General Catalog (AGC) ID, resulting in a total of 31,500 entries with 53 columns.

For the H I velocity width, I start with the reported velocity width at 20% level of each of the two peaks in the line profile (`W20`) in the $\alpha.100$ catalog (Haynes et al. 2018), because it is expected to capture more of the flat parts of a rotation curve than the 50% level velocity width (`W50`). All reported velocity widths are corrected for instrumental broadening following the simulations of Springob et al. (2005). `W20` are given in observed frame instead of in rest frame, and the rest-frame H I velocity widths (W_{20}) are obtained by dividing `W20` by $(1+cz_\odot/c)$, where $cz_\odot$ is the Heliocentric velocity of the H I profile (column `Vhelio` in the catalog).

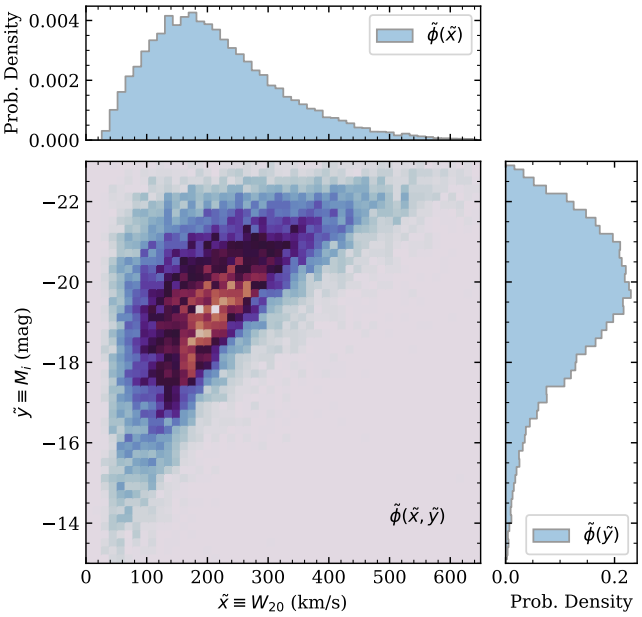

FIG. 1.— The distribution of ALFALFA-SDSS galaxies in the plane of i-band absolute magnitude vs. H I line width. This is the input $\tilde{\phi}(\tilde{x},\tilde{y})$ function, which will be rectified by the Lucy algorithm to *statistically* remove the effects from random disk orientations and random measurement errors. Here and in most of the subsequent figures, the main panel shows the 2D distribution, and the side panels show the marginalized distributions over each axis.

For the i-band absolute magnitude, I start with the `ABSMAG_I_CORR` column in the ALFALFA-SDSS galaxy catalog (Durbala et al. 2020). It is derived from SDSS i-band `cmodel` magnitude and has been corrected for both foreground Galactic extinction and internal dust extinction due to inclination. For the internal correction, the authors used the r-band axial ratio (b/a) from SDSS exponential model fits (`expAB_r`)[1] and a simple logarithmic formula for the internal extinction[2], $M_{i,\rm corr} = M_i + \gamma_i(M_i)\log(b/a)$, a parameterization originated from Eq. 27 of Giovanelli et al. (1994). Because magnitudes uncorrected for inclination is desired for this study, I reversed the internal extinction correction using the listed γ_i values in the catalog (`gamma_i`) and the relation the authors used to calculate γ_i from M_i: $\gamma_i = -0.15M_i - 2.55$ for $M_i < -17$. For less luminous galaxies with $M_i > -17$, M_i equals $M_{i,\rm corr}$ since $\gamma_i = 0$. After this process, the resulting M_i magnitudes are corrected for foreground Galactic extinction only.

Lastly, the uncertainties of the measurements are needed to construct the joint PDF in Eq. 1. In the ALFALFA-SDSS catalog, the estimated uncertainties on `W50` have a median at 9 km s^{-1} and a mean at 18 km s^{-1}, which are comparable to the spectral resolution of ALFA (10 km s^{-1} after Hanning smoothing, for a channel spacing of 5 km s^{-1}). The uncertainty of `W20` is not reported because they are difficult to quantify for the polynomial fitting algorithm, so I assume a similar uncertainty of 20 km s^{-1} for W_{20}. For the absolute

[1] Axial ratios are not used in this study.

[2] The additional internal extinction when viewed face-on is *not* corrected for in this formula.

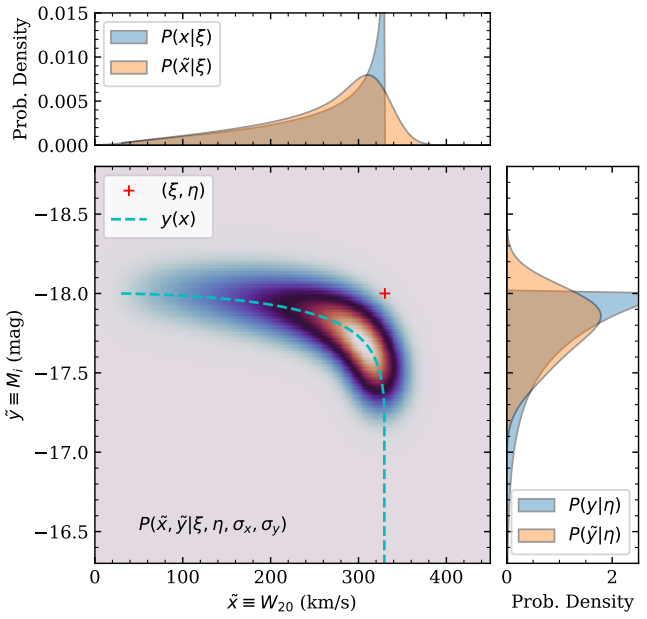

FIG. 2.— The joint PDF $P(\tilde{x},\tilde{y}|\xi,\eta,\sigma_x,\sigma_y)$ for $\xi = 330\,\mathrm{km\ s^{-1}}$, $\eta = -18$, $\sigma_x = 20\,\mathrm{km\ s^{-1}}$, $\sigma_y = 0.14$, $w_0 = 30\,\mathrm{km\ s^{-1}}$, and $\gamma = 0.73$. The intrinsic values are indicated by the *red cross*, which is offset from the peak of the PDF. The top panel shows the PDF marginalized over the $\tilde{y}$-axis (*yellow*). This gives the PDF of the measured values, $P(\tilde{x}|\xi,\sigma_x)$ per Eq. 13, which can be compared with the PDF of the true projected values $P(x|\xi)$ from Eq. 10 (*blue*) to see the effects of measurement errors. The right panel shows the joint PDF marginalized over the $\tilde{x}$-axis and $P(y|\eta)$ from Eq. 11.

magnitude M_i, I adopt the mean of the magnitude errors listed in `ABSMAG_I_CORR_ERR`, which is 0.14 mag. In summary, $\sigma_x = 20\,\mathrm{km\ s^{-1}}$, and $\sigma_y = 0.14$ mag.

A total of 28,264 sources (90% of the α.100 sample) in the merged catalog have valid velocity widths and absolute magnitudes, and that forms the galaxy sample for this study, because no further down-selection is necessary. Figure 1 shows the distribution of the sample in the plane of W_{20} and M_i as a 2D histogram. This represents $\tilde{\phi}(\tilde{x},\tilde{y})$ in Eq. 7.

3.2. *Joint Probability Density Function*

Both the H I velocity width and the absolute magnitudes are affected by the inclination angle i of the disk galaxy because of projection effects. The true projected values and the intrinsic values follow these simple relations:

$$x = \sqrt{(\xi \sin i)^2 + w_0^2} \tag{8}$$

$$y = \eta - \gamma \log(\cos i) \tag{9}$$

where the inclination angle i is defined to be zero when viewed face-on and 90° when viewed edge-on. In Eq. 8, the projected velocity width is expressed as the quadrature sum of the line-of-sight projection of the edge-on velocity width and the velocity width from random motions (w_0). I set $w_0 = 30\,\mathrm{km\ s^{-1}}$ based on the lower boundary in the observed distribution of velocity widths in Figure 1.

In Eq. 9, the projected absolute magnitude follows the parameterization in Eq. 27 of Giovanelli et al. (1994), which fits well the observed inclination dependency of M^* (the knee of the optical luminosity functions) for low-z disk galaxies in the five SDSS filters (Shao et al. 2007). As expected from the dust extinction curve, the extinction coefficient γ decreases as wavelength increases. Here I adopt the γ value for SDSS i-band from Shao et al. (2007) ($\gamma_2 = 0.73 \pm 0.04$ in their Table 4). To interpret the meaning of γ, one can compare the extinction term above, $A = \gamma \log(\sec i)$, with the plane-parallel extinction, $A' = 2.5\log(e)\tau_0(\sec i - 1)$, where $\tau_{0,\lambda}$ is the face-on optical depth of the disk. At the face-on limit, $i \to 0$ or $\sec i \to 1$, the coefficient γ is simply 2.5× the face-on optical depth: $\gamma = 2.5\tau_0$. So $\gamma = 0.73$ implies an optical depth of $\tau_0 = 0.29$, and face-on disks become optically thick when $\gamma > 2.5$.

Assuming the disks are randomly oriented on the sky, the PDF of the inclination angle is $P(i) = \sin i$. Given this and the relations in Eqs. 8-9, the conditional PDF of x and y are:

$$P(x|\xi) = \frac{x/\xi}{\sqrt{\xi^2 - (x^2 - w_0^2)}} \text{ when } 0 \le x \le \xi \tag{10}$$

$$P(y|\eta) = \frac{\ln 10}{\gamma} 10^{(\eta - y)/\gamma} \text{ when } \eta < y \tag{11}$$

In addition, since both x and y are related to the inclination angle i, the two are correlated:

$$y = \eta - 0.5\gamma \log(1 - \frac{x^2 - w_0^2}{\xi^2}) \tag{12}$$

The joint conditional PDF of x and y is determined by Eqs. 10-12 because when integrated over one axis it must recover the conditional PDF of the other axis:

$$\int P(x,y|\xi,\eta)dy = P(x|\xi) = \frac{x/\xi}{\sqrt{\xi^2 - x^2}} \tag{13}$$

$$\int P(x,y|\xi,\eta)dx = P(y|\eta) = \frac{\ln 10}{\gamma} 10^{(\eta - y)/\gamma} \tag{14}$$

The correlation relation in Eq. 12 explains why η drops off after the integral in Eq. 13 and ξ drops off in Eq. 14, since this additional equation allows η or ξ to be expressed by the other three parameters.

All measurements have errors, and the errors scatter the measured value around the true value following a PDF that is usually assumed to be Gaussian. Because the velocity widths and the absolute magnitudes come from two different surveys (ALFALFA and SDSS), and only the latter depends on the distance to the source, we can safely assume that the measurement errors in x and y are uncorrelated. As a result, the error PDF is a 2D Gaussian with major and minor axes aligned with the x and y axes:

$$G(x - \tilde{x}, y - \tilde{y}|\sigma_x,\sigma_y) = \frac{1}{2\pi\sigma_x\sigma_y} \exp\left(-\frac{(\tilde{x}-x)^2}{2\sigma_x^2}\right) \exp\left(-\frac{(\tilde{y}-y)^2}{2\sigma_y^2}\right) \tag{15}$$

And the joint conditional PDF of $\tilde{x}$ and $\tilde{y}$ is then $P(x,y|\xi,\eta)$ convolved with the 2D Gaussian:

$$P(\tilde{x},\tilde{y}|\xi,\eta,\sigma_x,\sigma_y) = \iint P(x,y|\xi,\eta)G(x-\tilde{x}, y-\tilde{y}|\sigma_x,\sigma_y)dxdy \tag{16}$$

Efficient convolution algorithms based on Fast Fourier Transform (FFT) can be used to evaluate $P(\tilde{x},\tilde{y}|\xi,\eta,\sigma_x,\sigma_y)$ on the $\tilde{x},\tilde{y}$ plane for a grid of ξ,η. Over the parameter ranges covered by the data, $0 < x < 650\,\mathrm{km\ s^{-1}}$ and $-23 < y < -12$, I calculate the joint PDF on a 51×51 grid in both $(\tilde{x},\tilde{y})$ and (ξ,η) with spacings of $13\,\mathrm{km\ s^{-1}}$ and 0.2 mag. The resulting

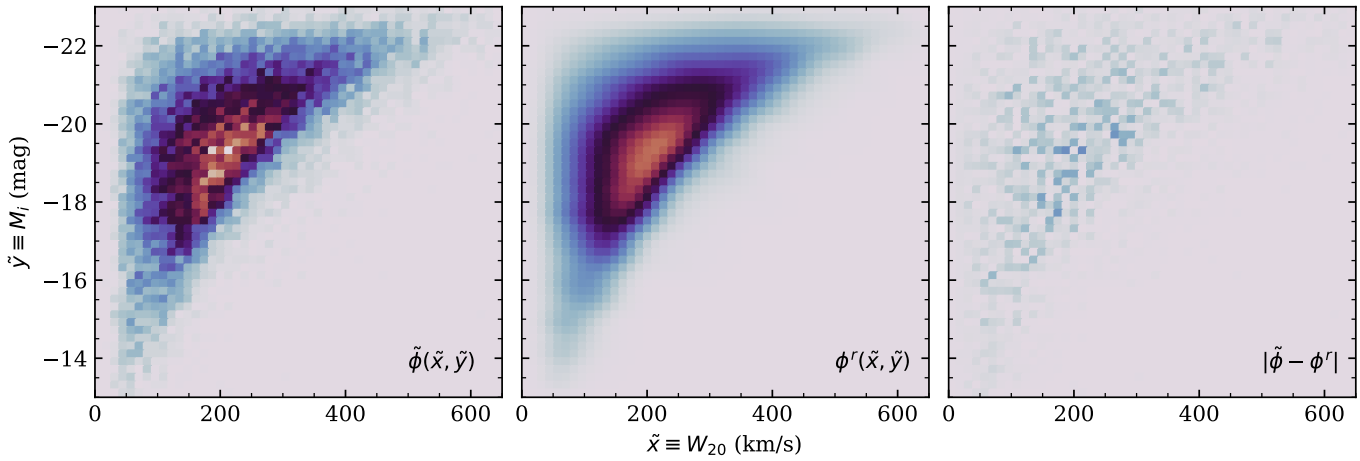

FIG. 3.— Data vs. model. From left to right are respectively the observed $\tilde{\phi}$ distribution (same as Fig. 1), the model ϕ^r distribution after 30 iterations, and the absolute differences between the two distributions. For fair comparison, the same color scale and contrast are used in all panels.

4D array can be interpolated and used for integrations in the iterative process (Eqs. 6 and 7).

Figure 2 shows an example of the joint PDF. As expected, the population is dominated by more inclined disks, which show higher velocity widths but suffer more internal dust extinction. The correlation between the axes (Eq. 12) is also evident. As described in §3.1, I estimated the mean measurement errors to be $\sigma_x = 20\,\mathrm{km\ s^{-1}}$ and $\sigma_y = 0.14$ mag. An accurate knowledge of the measurement errors only matters when one desires to quantify the intrinsic dispersion of the recovered relation, because if the errors were underestimated (overestimated), the recovered intrinsic distribution would have shown a larger (smaller) scatter.

3.3. *Recovered Intrinsic Distribution*

To start the iterative process, one needs to prescribe an initial distribution for $\psi(\xi,\eta)$. Usually it is recommended to prescribe the observed distribution as the initial guess, $\psi^0(\xi,\eta) = \tilde{\phi}(\tilde{x},\tilde{y})$, to speed up the convergence. But because the position of the intrinsic position is offset from the peak of the joint PDF, as illustrated in Figure 2, one would expect similar offsets between ψ and ϕ. So I simply prescribed a flat distribution as the initial guess, $\psi^0(\xi,\eta) =$ constant, over the parameter ranges covered by the data, $0 < \xi < 650\,\mathrm{km\ s^{-1}}$ and $-23 < \eta < -12$, on a 51×51 grid with spacings of $13\,\mathrm{km\ s^{-1}}$ and 0.2 mag.

At the end of each iteration, both the rectified distribution $\psi^r(\xi,\eta)$ (Eq. 7) and its corresponding projected distribution $\phi^r(\tilde{x},\tilde{y})$ (Eq. 6) are produced. The latter can be directly compared with the observed distribution $\tilde{\phi}(\tilde{x},\tilde{y})$ to assess the improvement of the model after each iteration. As already noted in previous works, the Lucy algorithm is very efficient. After just a few iterations, a narrow curved distribution begins to emerge in ψ^r and the resulting ϕ^r starts to converge onto the input $\tilde{\phi}$. Based on the residual map $(\tilde{\phi}-\phi^r)$ and the expected Poisson noise of $\tilde{\phi}$, I find that the reduced χ^2_ν decreases from 13.7 after the first iteration to 1.0 after 30 iterations, which is a natural point to stop the algorithm. Figure 3 shows that the model distribution after 30 iterations accurately reproduces the observed distribution, and there is only statistical noise left in the residual map.

Figure **??** shows the rectified distribution after 30 iterations. The main panel shows that $\psi^r(\xi,\eta)$ is confined to a narrow, continuous sequence along the diagonal direction, revealing a tight correlation between the *edge-on* H I line width and the *face-on* *i*-band absolute magnitude of H I-selected galaxies. This is the *i*-band Tully-Fisher relation from the full sample of 28,264 H I-selected nearby ($z < 0.06$) galaxies in the ALFALFA-SDSS catalog. Note that because the full sample is used (as opposed to selecting only high inclination disks as in previous studies), the absence of any significant secondary trend in the intrinsic distribution shows that the overwhelming majority of H I-selected galaxies follow a single Tully-Fisher relation.

The Tully-Fisher relation is usually parameterized as a power law between luminosity and velocity-width: $L \propto W^\beta$. Since magnitude is used here, the relation translates to $M_i = M_0 - 2.5\beta\,[\log(W/250\,\mathrm{km/s})]$, where β is the slope and M_0 is the intercept point at $250\,\mathrm{km\ s^{-1}}$. To determine these parameters, I fit the power-law relation to the ridge in the rectified distribution $\psi^r(\xi,\eta)$. First, I measure the width of the ridge and the location of its peak at each fixed M_i by fitting a Gaussian function to each row of the 2D distribution. Then, the same measurements are made at each fixed W_{20} by fitting each column. Finally, the power-law model is fit to the two sets of ridge peak measurements, using the Gaussian σ widths as relative errors. Similar M_0 values are found from both measurement sets, but the slopes differ: $\beta = 4.39 \pm 0.06$ and 3.78 ± 0.03 from by-row and by-column measurements, respectively. I take the mean of the two best-fit values and use their difference as twice the error. The resulting Tully-Fisher relation is:

$$\begin{aligned} M_{i,\mathrm{face-on}} &= M_0 - 2.5\beta \log\left(\frac{W_{20,\mathrm{edge-on}}}{250\,\mathrm{km/s}}\right) \\ M_0 &= -19.77 \pm 0.04 \\ \beta &= 4.1 \pm 0.3 \end{aligned} \tag{17}$$

Both the horizontal and the vertical widths of the ridge are roughly constant in logarithmic scales, with the median Gaussian σ values of $\sigma(\log W) = 0.07$ dex and $\sigma_M = 0.5$ mag. These should be considered as the upper limits on the intrinsic dispersion of the Tully-Fisher relation, because there could be additional measurement errors that are not included in the joint PDF.

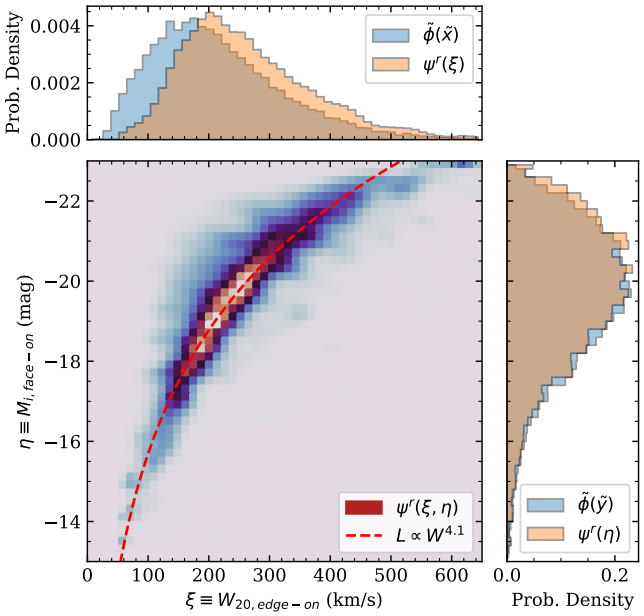

FIG. 4.— The rectified distribution $\psi^r(\xi,\eta)$ after 30 iterations. The red dashed curve in the main panel shows the best-fit Tully-Fisher relation in Eq. 17. The side panels compare the marginalized distributions before and after rectification (*blue* and *yellow*, respectively). They illustrates the differences between the observed H I-velocity width function and *i*-band luminosity function and the inclination angle corrected counterparts. Note that selection effects such as the magnitude limit and the volume incompleteness have not been corrected.

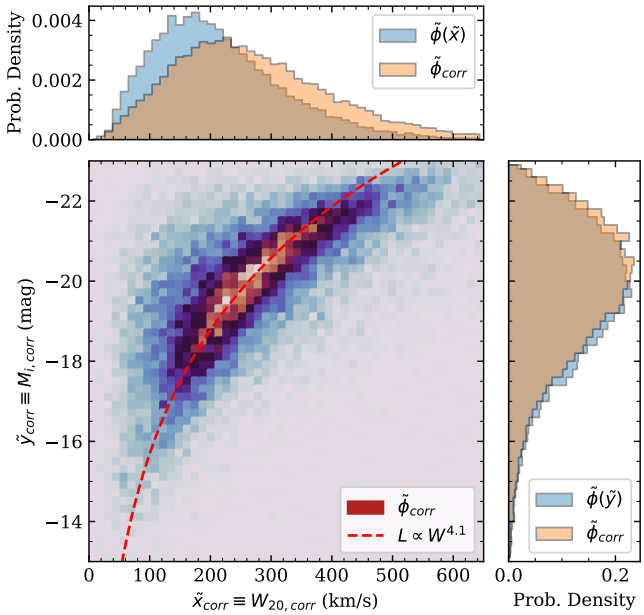

FIG. 5.— The distribution of the ALFALFA-SDSS galaxy sample after individual inclination angle correction based on the axial ratio (b/a). Same as in Fig. 4, the red dashed curve shows the Tully-Fisher relation in Eq. 17 and the side panels compare the marginalized distributions before and after the inclination-angle correction.

Marginalized over each axis, the rectified distribution $\psi(\xi,\eta)$ provides the edge-on H I velocity-width function and the face-on *i*-band luminosity function of H I-selected disk galaxies. Of course, both functions are still modified by the uncorrected selection effects such as the magnitude limit, the line detection limit, and the volume incompleteness. The face-on luminosity function is simply shifted by $\sim$0.2 mag towards to brighter end. The changes in the velocity-width function are more pronounced. After the rectification, not only its peak shifts by $\sim$50 km s^{-1} to the higher end, but also its slopes on both sides of the peak become steeper.

3.4. *Comparison with conventional method*

Having successfully revealed the Tully-Fisher relation through rectification, in this subsection I compare the results with the traditionally adopted method in studies of the Tully-Fisher relation, which is to carry out inclination correction to individual galaxies using the observed axial ratios from optical imaging data. The procedure is straight-forward. First, one estimates $\sin i$ of each galaxy using the following equation:

$$\sin^2 i = \frac{1-(b/a)^2}{1-q_0^2} \tag{18}$$

where q_0 is the *assumed* edge-on axial ratio of the disk. Next, one corrects the projection effects in both the observed velocity width and the observed absolute magnitude using the estimated inclination angle for each galaxy:

$$\begin{aligned} W_{20,\rm corr} &= \sqrt{W_{20}^2 - w_0^2}/\sin i \\ M_{i,\rm corr} &= M_i + \gamma \log(\cos i) \end{aligned} \tag{19}$$

which are simply the reversed relations of Eqs. 8 and 9. Finally, one generates the 2D histogram using the individually corrected values.

I proceed to carry out the individual corrections to the ALFALFA-SDSS sample. To estimate the inclination angles, I assume $q_0 = 0.15$ and adopt the *r*-band axial ratio from SDSS exponential model fits (Column `expAB_r`). For the corrections, I assume $w_0 = 30$ km s^{-1} and $\gamma = 0.73$ to be consistent with the rectification analysis. For the *i*-band absolute magnitude, I get essentially the same result if I simply use the inclination corrected values (column `ABSMAG_I_CORR`) in the ALFALFA-SDSS catalog. Fig. 5 shows the resulting distribution using the corrected velocity widths and absolute magnitudes. This figure should be directly compared with Fig. 4. Although both results are consistent with the same $\beta = 4$ power law relation, the differences between the conventional method of individual correction and statistical rectification are quite easy to tell. There are substantial populations of "outlier" galaxies that seem to be either under-corrected or over-corrected in the traditional method. And probably due to these outliers, the corrected velocity-width function is significantly less sharply peaked than that from the rectification method. The corrected Tully-Fisher relation also appears much broader than that from the rectification method, likely because the measurement errors are not corrected in the traditional method.

The comparison above clearly shows that better results can be obtained using the statistical rectification method. Now I briefly discuss why this is the case. When compared with the statistical rectification method introduced in this work, the main disadvantages of the traditional method include:

1. One additional measurement set, the axial ratio b/a, must be used to estimate $\sin i$;

2. Measurement errors are not corrected for.

The former introduces another source of error and may not be available or reliable if the angular sizes of galaxies are small compared to the spatial resolution. The latter makes the resulting Tully-Fisher relation broader, which in turn makes it more difficult to quantify the intrinsic scatter of the relation. The former is especially important, and it is the main reason causing the differences in the results. Eq. 18 was first derived by Hubble (1926), who assumed disk galaxies were axisymmetric oblate ellipsoids. One faces two main problems when using this equation to estimate the inclination angle:

1. The edge-on axial ratio, q_0, is not well determined and likely varies with morphological type; the literature has assumed values between $0.1 \leq q_0 \leq 0.2$ (e.g., Giovanelli et al. 1994; Xilouris et al. 1999; Ryden 2006).

2. Disk galaxies are not axisymmetric. Instead, they show median ellipticity between $0.07 \leq \epsilon \leq 0.18$ (Ryden 2006).

For these reasons, previous Tully-Fisher relation studies have excluded galaxies with low inclination angles to minimize the amount of correction to the velocity widths (e.g., $\sin i > 0.87$ when $i > 60^\circ$). But this exclusion alone would severely reduce the sample size; e.g., the ALFALFA-SDSS galaxy sample would be reduced by a factor of three when I exclude galaxies with $i < 60^\circ$.

4. SUMMARY AND FUTURE PROSPECT

The Tully & Fisher (1977) relation is an important empirical correlation between the edge-on rotation velocity and the face-on luminosity of disk galaxies. To determine this relation, three sets of observed properties are typically required: galaxy-integrated line widths (W), absolute magnitudes (M), and the axial ratios (b/a). The axial ratios are needed because the first two observed properties needed to be corrected for the inclination angle (i) of the disk. One major issue of this approach is that the b/a-based individual inclination correction introduces additional errors to the corrected properties, because (1) the edge-on axial ratio as a function of luminosity have not been precisely measured for disk galaxies, (2) disk galaxies deviate from the assumed axisymmetric oblate ellipsoid model, and (3) axial ratios from different techniques differ (e.g., morphological fitting vs. isophotes) and are affected by atmospheric seeing. To minimize the impact of b/a-based inclination correction, low-inclination disks have been excluded from previous studies. This exclusion not only severely reduces the sample size (thus the statistical accuracy of the result), but also made it impossible to assess whether the excluded sample follows the same relation as the included sample. The requirement of b/a measurement also made it hard to apply the technique to higher redshifts, because these galaxies are usually not well resolved.

In this work, I have demonstrated a rectification technique that replaces *individual* inclination correction with *ensemble* statistical correction. It determines the Tully-Fisher relation with only two sets of observables (W and M) and utilizes the full sample of disk galaxies regardless of their inclination angles. The following describes the general philosophy. When the observed properties can be converted from the intrinsic properties and the inclination angles with some known relations, one can predict joint PDF of the observed properties by assuming randomly oriented disks and random measurement errors. The recovery of the distribution of the intrinsic properties from the distribution of observables then becomes a reversal of *the law of total probability* in Eq. 1 that can be tackled numerically with the iterative rectification algorithm of Lucy (1974).

With 28,264 H I-detected disk galaxies from the ALFALFA-SDSS survey at $z < 0.06$, I show that the rectified distribution of *edge-on* H I line width and *face-on* i-band absolute magnitude of H I-selected disk galaxies follows a sharp power-law relation, $M_i = -19.8 - 2.5\beta\,[\log(W_{20,\rm HI}/250{\rm km/s})]$, with $\beta = 4.1 \pm 0.3$ and intrinsic dispersions of $\sigma_W \lesssim 24$ km s^{-1}and $\sigma_{M_i} \lesssim 0.5$ mag. The absence of any significant secondary trends in the rectified distribution shows that all H I-selected disk galaxies follow a single Tully-Fisher relation. In addition, the rectified distribution marginalized over each axis provides the inclination-corrected H I velocity width function and the luminosity function of these galaxies, both of which show significant changes from the observed functions.

The statistical rectification technique can be applied to a wide range of astrophysical problems, as long as (1) the observed properties can be converted from the intrinsic properties by a relation that involves a "hidden" parameter (e.g., i) and (2) the hidden parameter is unobserved but its PDF is precisely known. In future studies of disk galaxies, the technique can be used to determine not only the Tully-Fisher relation and the inclination-corrected luminosity function and velocity width function at high redshift (where no reliable axial ratio measurements are available), but also the edge-on thickness (c/a) and face-on ellipticity (ϵ) of disk galaxies as a function of absolute magnitude (i.e., extending the work of Binney & de Vaucouleurs 1981; Vincent & Ryden 2005; Ryden 2006; Roychowdhury et al. 2010). The potential grows stronger with the increasing number of astronomical surveys generating statistical datasets encompassing samples of galaxies.

I thank my colleagues Steve Spangler, Ken Gayley, and Kevin Hall for helpful conversations. This work is supported by the National Science Foundation (NSF) grant AST-2103251.

REFERENCES

Ball, C. J., Haynes, M. P., Jones, M. G., et al. 2023, ApJ, 950, 87
Binney, J., & de Vaucouleurs, G. 1981, MNRAS, 194, 679
Cornwell, T. J. 2009, A&A, 500, 65
Desmond, H. 2017, MNRAS, 472, L35
Durbala, A., Finn, R. A., Crone Odekon, M., et al. 2020, AJ, 160, 271
Giovanelli, R., Haynes, M. P., Salzer, J. J., et al. 1994, AJ, 107, 2036
Haynes, M. P., Giovanelli, R., Kent, B. R., et al. 2018, ApJ, 861, 49
Högbom, J. A. 1974, A&AS, 15, 417
Hubble, E. P. 1926, ApJ, 64, 321
Lucy, L. B. 1974, AJ, 79, 745
Orieux, F., Giovannelli, J.-F., & Rodet, T. 2010, Journal of the Optical Society of America A, 27, 1593
Richardson, W. H. 1972, Journal of the Optical Society of America (1917-1983), 62, 55
Roychowdhury, S., Chengalur, J. N., Begum, A., & Karachentsev, I. D. 2010, MNRAS, 404, L60
Ryden, B. S. 2006, ApJ, 641, 773
Shao, Z., Xiao, Q., Shen, S., et al. 2007, ApJ, 659, 1159
Springob, C. M., Haynes, M. P., Giovanelli, R., & Kent, B. R. 2005, ApJS, 160, 149
Tiley, A. L., Bureau, M., Saintonge, A., et al. 2016, MNRAS, 461, 3494
Topal, S., Bureau, M., Tiley, A. L., Davis, T. A., & Torii, K. 2018, MNRAS, 479, 3319
Tully, R. B., & Courtois, H. M. 2012, ApJ, 749, 78
Tully, R. B., & Fisher, J. R. 1977, A&A, 54, 661
Vincent, R. A., & Ryden, B. S. 2005, ApJ, 623, 137
Xilouris, E. M., Byun, Y. I., Kylafis, N. D., Paleologou, E. V., & Papamastorakis, J. 1999, A&A, 344, 868

Zaritsky, D., Courtois, H., Muñoz-Mateos, J.-C., et al. 2014, AJ, 147, 134